TDA Progress Report 42-114

August 15, 1993

Stability Measurements of the Radio Science System at the 34-m High-Efficiency Antennas

T. T. Pham, J. C. Breidenthal, and T. K. Peng
Telecommunications Systems Section

S. F. Abbate and S. T. Rockwell
TDA Mission Support and DSN Operations

From 1991 to 1993 the fractional frequency stability of the operational Radio Science System was measured at DSS's 15, 45, and 65. These stations are designed to have the most stable uplink and downlink equipment in the DSN. Some measurements were performed when the antenna was moving and the frequency was ramped. The stability, including contributions of all elements in the station except for the antenna and the hydrogen maser, was measured to be 0.3 to 1.3 × 10^{-15} when the frequency was fixed, and 0.6 to 6.0 × 10^{-15} when the frequency was ramped (sample interval, 1000 sec). Only one measurement out of fifteen exceeded specification. In all other cases, when previous measurements on the antenna and the hydrogen maser were added, a total system stability requirement of 5.0 × 10^{-15} was met. In addition, ambient temperature was found to cause phase variation in the measurements at a rate of 5.5 deg of phase per deg C.

I. Introduction

Good frequency stability is essential in the Radio Science System, since frequency is one of the primary observable parameters in radio science experiments. The required period of stability varies from a few hundred to several thousand seconds, depending on the nature of the experiment. For example, gravitational wave detection experiments usually require high two-way stability over a long round-trip light time between the Earth and a spacecraft. A 1000-sec duration is often used as a convenient checkpoint for the range of round-trip light time encountered in practice. On the other hand, for occultation studies, the time scale of interest is much shorter. All that is needed is stability over the time interval it takes a spacecraft to descend through the planetary atmosphere. For Mars Observer, this time scale is no more than 300 sec.

The focus of this investigation is the frequency stability performance of the open-loop Radio Science System at the 34-m high-efficiency (HEF) subnet. More interest is placed on this subnet, rather than the 70-m or 34-m standard (STD), because of the HEF's inherently greater stability. This greater stability results from a deliberate attempt during design to capitalize on the fact that phase scintillation due to the solar wind and Earth's ionosphere decreases with the inverse square of the carrier frequency. For this reason, the 34-m HEF subnet was equipped with X-band (8.4 GHz) uplink and downlink equipment of stability better than the anticipated phase scintillation. The

potential 13-fold improvement compared to S-band-only (2.3-GHz) stations, and a ninefold improvement compared to S-band uplink/X-band downlink stations, makes the 34-m HEF stations the best available for detecting gravitational radiation by spacecraft tracking.

Specifically, the objectives of this study and their significance are as follows:

(1) *Stability performance in both one-way and two-way configuration.* One-way stability refers to that of the downlink equipment only, whereas two-way includes both uplink and downlink equipment. Knowledge of system performance in both one-way and two-way configurations is important due to the difference between gravitational wave and planetary atmosphere studies. The availability of both sets of measurements also helps to reveal the stability of the uplink path, which there is currently no way to directly measure.

(2) *Stability performance under both static and dynamic frequency conditions.* Static and dynamic conditions refer to cases where the test signal frequency is fixed and ramped, respectively. Static conditions are used frequently due to their compatibility with a simple test setup. However, measurement under dynamic conditions offers more insight on how the system performs in actual experiments. The signals received from spacecraft always have an associated Doppler frequency due to the relative velocity between the spacecraft and the tracking ground antenna. As the signal traverses the bandwidth that the Radio Science System operates prior to the point of Doppler compensation, it is distorted, however slightly, by the inherently dispersive electronic components in the system. At the point of Doppler compensation, the signal is again exposed to another form of degradation, caused by the potential phase instability of a programmable local oscillator. The objective of the dynamic test is to validate that such a distortion is small, as intended by the design.

(3) *Performance improvement due to the use of a low-thermal-coefficient fiber-optic link for antenna references.* With recent improvements, the 100-MHz references used in the exciter and the downconverter in the antenna area are transported from the Signal Processing Center (SPC) via a fiber-optic link. In the past, these references were transported via microwave coaxial cables and phase-stabilized cables. It should be noted that system measurements with either fiber-optic or phase-stabilized references do not include the contribution of the reference link because of the cancellation that results from using a common cable for both the uplink and downlink. These system tests are therefore limited to validating the function of the reference link. In order to account for the contribution of the hydrogen maser clock and the fiber-optic link in total system performance, the results from these tests are combined with those from stand-alone testing on the link itself. Section VI provides more details on this process.

(4) *Impact of the environment and operation on stability performance.* Particularly, the effect of antenna motion, radio frequency interference (RFI), diurnal temperature variation, and wind conditions are examined. Due to a limitation in the test configuration, to be discussed in Section II, the effect of antenna motion is only partially observed.

The foregoing objectives are intended to make a full characterization of the system, so that scientists will know the noise characteristics of the data they receive. It is worth noting that there were other similar studies on stability performance of the DSN equipment conducted and reported in earlier issues of *The Telecommunications and Data Acquisition Progress Report.* For example, Otoshi and Franco have published a series of extensive studies regarding the stability of a research and development (R&D) 34-m antenna at Goldstone (DSS 13) [1]. In 1989, in an effort to prepare for Voyager's Neptune encounter, Ham et al. conducted a series of stability measurements of the Radio Science System at Canberra's 70-m antenna (DSS 43) [2]. The present study shows a lot of commonality with those earlier efforts in terms of test configuration and instrumentation. However, there are also differences. Compared to [1], the present measurements reflect the stability at an operational 34-m HEF station, rather than at an R&D site. The equipment under test is the X-band uplink and radio science X-band downlink system. In contrast to [2], where stability is characterized at S-band with an S-band uplink system at the 70-m antenna, this study presents measurements at X-band. Also, the link between the SPC and the antenna is a fiber-optic link, instead of another transport medium. Lastly, the presented measurements include a more realistic performance with uplink Doppler simulation.

In the following sections, more details of this study are given. Section II provides a description of the test configuration. Section III presents the data acquisition and processing. Measurements and performance analysis are discussed in Sections IV and V. A conclusion is drawn in Section VI regarding whether the DSN Radio Science System satisfies its stability requirements. The summary and conclusions are given in Section VII.

II. Test Configuration

Most of the tests were conducted at the 34-m HEF antenna at Goldstone (DSS 15). This particular deep space station was chosen as the site of study because of its proximity to JPL. The equipment design is identical at DSS 45 (Canberra) and DSS 65 (Madrid), and less extensive tests at these sites have verified the conclusions drawn from the DSS-15 tests. The test configuration is presented in Fig. 1.

A. General Configuration

In one-way measurements, a test signal of 8.4 GHz was generated from a 100-MHz reference in the antenna by a highly stable ×84 signal generator, which is essentially an ovenized ×84 frequency multiplier. The 8.4-GHz signal was injected into the downlink microwave system prior to the X-band maser at a point known as the "ranging coupler." In two-way measurements, an X-band uplink signal was generated by the exciter and was converted to a downlink frequency by the test translator.

Once injected into the downlink system, the test signal was amplified by the X-band maser and later converted to 300 MHz intermediate frequency (IF) by the very long baseline interferometry/radio science (VLBI/RS) downconverter. The 300-MHz IF signal was transported from the antenna to the signal-processing center via a hard-line cable. The Radio Science IF-video downconverter (RIV) further converted the signal to baseband frequency. This downconversion process was achieved over several stages wherein the noise bandwidth was gradually reduced by various filters. In the first stage, any simulated Doppler, if present, was taken out by a programmable local oscillator. A small frequency offset was also introduced into this oscillator to place the carrier at a chosen position in the bandwidth of the equipment about to be described. In the final stage, a set of filters allowed six different bandwidth selections, ranging from 100 Hz to 20 kHz. At this point, the signal could be either channeled to the prototype stability analyzer for real-time stability measurement or to the Deep Space Communications Complex (DSCC) Spectrum Processing Subsystem (DSP) to be digitized and recorded on magnetic tapes for later processing. All stages of frequency conversion, both on the uplink and downlink paths, are depicted in Fig. 2.

In order to minimize thermal noise effects, test signals were set at a high power level but without saturating the low-noise amplifier. Typically, a signal-to-noise spectral density ratio of 60 dB-Hz or greater was used. A bandwidth of 100 Hz or 400 Hz in the final filtering was chosen to maximize the signal-to-noise ratio (SNR). Another benefit associated with the small bandwidth is the correspondingly small data volume, which helps to minimize the data extraction effort.

B. Antenna Frequency References

Of particular interest is the fact that a fiber-optic link is used to transport the 100-MHz references to the antenna area. These references are required by the exciter, test translator, VLBI/RS downconverter, and ×84 signal generator. This fiber-optic link includes a transmitter, receiver, low thermal coefficient-of-delay (LTCD) fiber-optic cable, and a 1-to-4 distributor. A prototype unit was made available during the engineering testing period by the Frequency and Timing Subsystem (FTS) Group, and operational units were recently deployed at all 34-m HEF stations as the official configuration.

These references have a significant impact on the overall stability of the system. Large frequency multiplication applied to these references (e.g.,×65 in the exciter and ×81 in the VLBI/RS downconverter, see Fig. 2) tends to amplify small frequency and phase fluctuations caused by the link between SPC and the antenna. Care must be taken to ensure that the link itself does not significantly degrade the stability of FTS references coming from the hydrogen maser. This concern is particularly appropriate considering the long distance that the link traverses—300–550 m, depending on the station—and the relatively large daily thermal fluctuation to which it is subjected.

The advantage in using fiber optics is twofold: a better performance in both long-term frequency stability and short-term spectral purity. In the earlier DSN configuration, a combination of coaxial hard lines and phase-stabilized cables were used for reference transmission. Although each had its own merit—high stability for the phase-stabilized cables and pure spectrum for hard lines—none offered the excellent performance in both aspects that fiber optics does. In the case of phase stabilization, the use of two frequency multipliers (i.e., ×4 and ×5) to convert a 5-MHz FTS reference to the desired 100 MHz resulted in an increase in phase noise, which was unacceptable for atmospheric and ring experiments. In the case of hard lines, stability performance was compromised by the rather large sensitivity to temperature variation that these cables have. Typically, the thermal coefficient of delay (TCD) of these microwave hard-line coaxial cables is about 15–18 ppm/deg C (parts per million per degree Celsius) for a temperature range of 18–33 deg C [3]. In contrast, the fiber-optic link directly transmits the 100-MHz reference without any up- or downconversion, and its TCD varies from 0.33 ppm/deg C to 0.83 ppm/deg C over the same temperature range [3].

Unfortunately, improvement with the use of fiber-optic link is not expected to be observable in the stability measurements. As indicated in Fig. 1, both uplink and downlink references are transported via a common link. Any phase variation caused by the fiber-optic link, or by the frequency and timing source, i.e., the hydrogen maser, would appear in both the generated test signal and the local oscillator of downconversion. Since there was essentially zero time delay between the uplink and downlink, the majority, 94 percent to be exact, of phase disturbance in the references was canceled. In other words, only 6 percent of fiber-optic stability appeared in the measurement. For this reason, the stand-alone measurement on the fiber-optic link done by Calhoun and Law[1] is used to augment the presented measurements in order to determine the total system performance.

Note that such cancellation does not apply to the measurements with non-zero round-trip light time, as in a real spacecraft tracking session, since the correlation in the phase of the incoming signal and the first local oscillator is then removed. In this case, the total stability is the root-sum square of contributions of the link and the rest of the system. As indicated in Calhoun and Law,[2] the stability contribution of the fiber-optic link was measured to be at least one-and-a-half orders of magnitude smaller than the rest of the system.

C. Antenna RF Cables

In the current system design, the RF cables that run across the antenna's moving parts are ring-wrapped to accommodate the antenna motion. As the antenna rotates to stay pointed to the target, physical stress is imposed on these cables. The stress can manifest itself in the form of abrupt phase discontinuity or a gradual phase drift. To study this impact, measurements were made with both a stationary and moving antenna.

D. IF Cables

The 300-MHz IF cables between the antenna and SPC, which deliver the downconverted signal to the RIV, are also a point of concern in terms of instability. A large portion of the cables not in the SPC or the antenna housing is exposed to a thermally unregulated environment. Temperature fluctuations, particularly around the period of sunrise and sunset, may have a severe impact on stability performance. Due to the relatively long time scale involved, the expected impact, if any, is likely in the form of gradual phase drift. Particular attention was paid in the data analysis to determine if there is any correlation between the variation in the temperature and the signal phase.

E. Limitations

There are inherent limitations associated with the test setup. The measurements did not account for frequency instability of the antenna or the standard hydrogen maser. The contribution of the antenna was excluded because there were no means to radiate a test signal onto the main reflector without a serious multipath interference problem. In addition, since both the test signal and the system under study were synchronized to the same frequency standard and the round-trip light time was zero, the coherence between them resulted in a near-perfect cancellation, making any frequency instability in the hydrogen maser unobservable.

Nevertheless, data on stand-alone tests on these two subsystems are available. For instance, Calhoun and Law[3] measured the two-way stability of the fiber-optic link and the hydrogen maser. Also, Otoshi recently reported a measurement of the antenna stability at the 34-m R&D station (DSS 13) in [4]. These two sets of data are used to augment measurements, thereby estimating total system performance.

III. Data Acquisition and Processing

Three different methods are currently available for data acquisition and processing, as depicted in Fig. 3. They will be referred to as complex demodulation, digital phase-lock loop (DPLL), and time interval. Both the complex demodulation and the DPLL methods rely on digitized voltage samples from the DSCC spectrum processor (DSP) subsystem. The time interval approach, however, uses the analog output from the receiver subsystem as input. Details on the data processing, as well as the strength and weakness of each method, are described below.

A. Complex Demodulation Method

The signal frequency is first estimated by applying a Fast Fourier Transform (FFT) operation on the incoming digitized samples. This estimated frequency is used as reference for the local oscillators that downconvert the signal

[1] M. D. Calhoun and J. C. Law, Communications and Systems Research Section, unpublished results on the stability of the fiber-optic distribution assembly (internal document), Jet Propulsion Laboratory, Pasadena, California.

[2] Ibid.

[3] M. D. Calhoun and J. C. Law, Communications and Systems Research Section, unpublished results on the stability of the fiber-optic distribution assembly and of the hydrogen maser/coherent reference generator (internal document), Jet Propulsion Laboratory, Pasadena, California.

to dc frequency. The downconversion is carried out in the complex domain, with both in-phase and quadrature arms. The outputs of the mixers are averaged over 1-sec intervals in order to enhance the SNR and to eliminate the double-frequency component. By taking the arc tangent of the ratio of the two averages, one can obtain the phase of the signal.

After the phase extraction process is completed, the phase samples are used as input into an algorithm that computes the Allan deviation in the phase domain. The computed Allan deviations serve as the measurement of system stability.

The advantage of this approach lies in its simplicity. Since the phase is estimated based on a one-second segment of the digitized samples and there is no feedback involved, the algorithm can tolerate a large variation in the input phase, up to 360 deg/sec. In contrast, the DPLL method that is described next requires a relatively small phase change among the input data. In the event of a large phase jump, either because of high noise level or missing data records, the loop will temporarily lose lock and require some time to re-establish the steady lock condition.

On the disadvantage side, the complex demodulation method requires the estimated frequency to be within 1 Hz of the true frequency. This is necessary to resolve the ambiguity in the phase determination as caused by the periodic tangent function.

In the process of calibration to understand how much noise the phase extraction process contributes, it was found that the algorithm, despite its simplicity, causes some degradation, particularly when the input signal frequency is fractional. The degradation comes from the fact that the 1-second averaging does not necessarily coincide with an integer number of cycles of signal, resulting in the twice-frequency component not being fully eliminated. The problem becomes more pronounced under low sampling-rate and high SNR conditions, which are often present in the testing.

B. Digital Phase-Lock Loop Method

The DPLL algorithm in use is based on [5], with major components presented in Fig. 3(b). The voltage input is first normalized to unity in amplitude by the automatic gain control (AGC) loop. The frequency deviation is extracted from the output of the loop filter at the rate of 1 sample per second. The frequency deviation can then be fed directly to an algorithm that computes the Allan deviation based on the frequency domain. Alternatively, the deviation can be converted from frequency to phase and input to a phase-domain Allan deviation algorithm as in the first method.

Note that the proper choice of PLL bandwidth is important. Selection of an improper loop bandwidth can cause a distortion in the test result. For example, a very small bandwidth, B_ℓ, will smooth out the detected phase variation, resulting in lower Allan deviations at those integration times less than $1/B_\ell$. A larger bandwidth, on the other hand, will allow more thermal noise leakage, creating an impression of high instability in the region where thermal noise dominates, i.e., up to roughly 100 sec. For data processing, a PLL bandwidth of 1 Hz is typically chosen for phase detection since the region of interest for stability performance lies between 1 second and several thousands of a second.

C. Time-Interval Method

With the first two approaches, data quality can only be evaluated at the end of data collection. The ability to monitor the performance of the system in real time is much desired. Such a capability is currently provided by a prototype model of the radio science stability analyzer, which is currently available at Goldstone.

The test setup for this method is shown in Fig. 3(c). The near-baseband analog signal taken out from the receiver is further downconverted by the analyzer to 1 Hz with a local synthesizer. The 1-Hz sinusoidal signal then gets low-pass filtered and transformed to a 1-pps (pulse-per-second) signal by the zero crossing detector. The time of the raising transition of the 1-Hz pulse is measured relative to the 10-pps "picket-fence" reference. Time interval measurements are converted to relative phases, from which the Allan deviations are calculated. A more detailed description on the signal processing aspect of this method is provided in [6].

Some consistency among all three methods is established in Table 1. Three sets of data collected at Goldstone DSS 15 on DOY 334/1990, DOY 177/1991, and DOY 027/1993 are shown. All tests were conducted under frequency-static conditions, i.e., no ramping in the uplink or downlink. Among the three methods, the average variation was about 50 percent, although there are cases where the difference exceeded the 100-percent level. This is not necessarily bad, considering there are measurements where a large fluctuation in the Allan deviation was observed at different integration times. These troublesome measurements will be pointed out later in the data analysis section. Note also that no single method consistently

produced higher or lower Allan deviations than the other two.

This consistency ensures that the data can be processed by any of the three methods discussed above. As it turns out, most of the test results were processed with the complex demodulation and DPLL methods, although only the data from the DPLL processing are presented here. Not many results associated with the time-interval method are available. The prototype stability analyzer, despite its great benefit as real-time test equipment, is a one-of-a-kind machine and is not available at the oversea stations. In addition, the analyzer does not handle well the testing of frequency dynamic conditions. This limitation comes from the fact that the input signal to the analyzer has a small frequency drift, typically around 30 μHz/sec. This drift is the result of imperfect compensation between the uplink and downlink ramps, due to finite resolution in the frequency rate register. The time-interval samples at the beginning and at the end of the test no longer span the same period (e.g., 1 sec), thereby invalidating the calculation of the Allan deviation. In contrast, the complex demodulation and DPLL methods can remove the residual frequency drift by tuning the local oscillators accordingly.

IV. Acquired Data

The presented measurements span two-and-a-half years. The study started with the preparation to support the then-anticipated X-band Gravitational Wave Experiment with Galileo, scheduled for April 1991. It was finalized with system performance testing for the support of the recent Mars Observer Coincidence (along with Galileo and Ulysses) Gravitational Wave Experiment, in March 1993. Table 2 presents both the test configuration of each measurement and the associated stability at representative integration periods. The results are grouped according to the objective of the tests, such as two-way static, one-way static, two-way dynamic, etc. Multiple measurements within each group, when available, are shown in order to demonstrate the repeatability, or lack thereof, among test results. Measurements with known hardware problems are not included. A more detailed analysis is provided in the next section.

V. Performance Analysis

Analysis is given in the order presented in Table 2.

A. Performance Under Frequency-Static Conditions

1. Two-way link. Figure 4 presents the stability measurements, in terms of Allan deviation, in two-way frequency-static configuration at all three complexes. The respective phase profiles are shown in Fig. 5. The measurables include the stability of the exciter, test translator, microwave plumbing, X-band maser, VLBI/RS downconverter, IF/video downconverter, narrow-band occultation converter (NBOC), spectrum-processor assembly (SPA), and system cables that run between subsystems. Note that the 20-kW transmitter (TXR) was not included in the test; however, as the data from DOY 032, 1993 at DSS 15 indicates, the TXR contribution is very small. Therefore, these measurements can be used to represent all equipment in the Radio Science System, excluding the FTS and the Antenna Mechanical Subsystem (ANT). For reference purpose, the theoretical thermal contribution based on a 1-Hz PLL bandwidth and 60 dB-Hz signal level, which is the nominal level of testing, is also shown.

Overall, the measurements appeared to be consistent across different complexes. Several comments can be made:

(a) At short integration times, i.e., less than 100 sec, the drop-off in the Allan deviation somewhat followed the $1/T$ relationship, where T is the integration time. Both DOY 035 and 067 had a slower drop-off rate between 10 and 100 sec, suggesting that there was an additional degradation factor involved. In fact, as indicated in Fig. 5, there were several short-term phase glitches associated with these two data sets.

(b) DOY 105 data exhibited regular oscillation at short integration time scales. In the process of calibrating the algorithm, it was found that such oscillation can be caused by short-term phase bursts; however, the phase profile of this data set, as seen in Fig. 5, did not reveal any outstanding short bursts. Whether the cyclic nature of the phase toward the end of the test is responsible for the oscillation in the Allan deviation requires further investigation.

(c) At long integration times, i.e., 1000 sec or greater, three sets of measurement on DOY 035, DOY 067, and DOY 105 showed a consistently good stability performance at the level of 8.0×10^{-16}. This indicates that there was little noise contribution from electronic components in the system. The data from DOY 341 and DOY 027 showed a higher level of instability at these long periods. The change in the phase slope on DOY 341, which corresponded to a 300-μHz frequency jump and occurred three hours into the test, was partly responsible for the drift. The phase profile of DOY 027 also suggests that there was a frequency jump on the order of 70 μHz during the last hour of the test.

2. Stability of the transmitter. Figure 6 presents the measurements with and without the transmitter on the same day (DOY 032, 1993 at DSS 15).[4] The two plots lie practically on top of each other, indicating that the TXR contribution is insignificant. At 1000-sec integration, the measurement without the TXR was actually lower than that with the TXR; however, due to the small set of data samples, the uncertainty associated with this point was rather large.

3. One-way stability. One-way stability includes all contributions from downlink elements, ranging from the microwave to the DSP Subsystem. The result also includes the stability of the test signal source, namely the ×84 signal generator; however, its contribution was so small, e.g., 1.8×10^{-14} (1 sec), 3.0×10^{-15} (10 sec), 4.9×10^{-16} (100 sec), 1.6×10^{-16} (1000 sec), that it could be practically ignored.

Two data sets were collected on DOY 114 and DOY 087, 1992 at DSS 15. The Allan deviation and associated phase profiles are shown in Figs. 7 and 8, respectively.

The stability measurement on DOY 114 shows a hump at the integration period between 200 and 1000 sec. It is believed to be associated with a steep phase slope, i.e., frequency jump, as indicated in Fig. 8. It is unknown whether such a frequency jump occurred in the ×84 signal generator or the downlink system. Despite such a peculiar appearance, the stability performance is very good, down to the 4×10^{-16} level at 1000-sec integration.

Both stability measurements on DOY 114 and DOY 087 show a cyclic appearance. The cause is not yet identified since the phase profiles do not indicate any particular feature that may result in such oscillation.

B. Stability Performance Under Frequency-Dynamic Conditions

Measurement under frequency-dynamic conditions is limited to two-way testing. One-way measurement is not possible because the ×84 signal generator only generates a fixed signal at 8400 MHz. In these measurements, the frequency of the signal coming into the X-band maser was increased at an arbitrary rate of 0.94 Hz/sec, a dynamic that is comparable to what is received from spacecraft.

Figure 9 shows the measured stability on DOY's 019 and 068, 1991 at DSS 15, and DOY 340, 1992 at DSS 45. Among these three measurements, DOY 340 represented the best and DOY 068 the worst.

For DOY 340, the Allan deviation at 1000 sec was comparable with those measured under static conditions (see Fig. 4). At shorter integration, the DOY 340 result was somewhat higher. Oscillation in the Allan deviation was observed, but the cause is unknown.

For DOY 019, the stability was not as good. The Allan deviation was about three time larger than the static test on DOY 105, i.e., 1.985×10^{-15} instead of 7.30×10^{-16}. Several phase glitches on the order of 5 to 10 degrees were observed, as seen in Fig. 10(a).

For DOY 068, the 1000-sec Allan deviation was as high as 5.9×10^{-15}, which exceeded the system requirement. This high level of instability was believed to be caused by the changes in the signal frequency, as indicated by the three phase segments of different slopes in Fig. 10(b). A large phase glitch on the order of 90 deg was also observed at 5:56 GMT.

What could cause the frequency glitches observed on DOY 068? It is believed that the programmable synthesizer, either in the uplink or downlink path, was responsible, rather than the phase ripple in the front-end filtering. Had they been caused by the filter profiles, this phenomenon would have been observed in the other two tests on DOY 019 and DOY 340. Future testing under this configuration would be able to verify this conjecture.

One clarification is needed regarding the data processing of DOY 068. A corruption in the data extraction process made the digitized samples of the original data records not available for a period between 5:26 and 5:54 GMT. This problem forced consideration of either using only half of the collected data—before or after the gap—or joining the two segments and treating them as if no gap had occurred. The first option would have rendered the results with a higher uncertainty, due to smaller sample sets. The second option would have reduced the uncertainty associated with the computed Allan deviations at long integration times, but it required an assumption that the gap statistic was the same as the rest of the data set. The presented data were processed with the second option.

C. Effect of Frequency References at the Antenna

Figure 11 presents measurements made with three different media used to transport the frequency references to the antenna, namely hard line coaxial, phase-stabilized, and fiber-optic cables.

[4] D. Howell, Telecommunications Systems Section, unpublished test results (internal document), Jet Propulsion Laboratory, Pasadena, California.

1. Comparison with hard lines. In the earlier configuration, where the hard line cables were used to transport the antenna references, a separate link was used for the uplink and downlink references. Therefore, the link contribution was included in the system measurement, rather than canceled, as in the case of single-link fiber-optic or phase-stabilized cables. As seen in Fig. 11, the stability at 1000 sec for the hard line measurement was about 2.5 times greater than the fiber-optic measurement. The difference at short integration times is believed to be caused by different SNR settings between the two tests.

Note that a fair comparison required that a two-way contribution of the fiber-optic link be included in the fiber-optic measurement. However, since the contribution of the fiber-optic link is an order of magnitude smaller than the actual measurement for the rest of the system, the sum of the two factors, in the mean square sense, can be approximated by the actual measurement.

2. Comparison with phase-stabilized cables. In the configuration associated with fiber-optic and phase-stabilized references, a common link was used to transport the antenna references. Because of this, one would have expected both measurements to yield the same performance because the link contribution is not observable. Surprisingly, the results indicated otherwise. Fiber-optic measurement on DOY 035, 1993 was about 60 percent better than the phase-stabilized measurement on DOY 014, 1991 over the range of 1000–3600 sec of integration.

D. Impact of Antenna Motion

The primary impacts of the antenna pointing, such as surface deformation due to gravity, imperfect compensation to the loading by the subreflector, etc., are not observable in the test setup. However, some secondary effects should be observable. These include the vibration imposed on the assemblies that are housed in the antenna cone, and the stress on the RF cables that run between the antenna tilting room and the pedestal. The vibration, if large enough, should show up as periodic variation at the frequency of vibration. Cable stress, on the other hand, would be more likely to manifest itself as a fast linear phase drift. Such a drift, on the order of 70 deg over 500 sec, had been observed by Rebold[5] when the antenna was driven at maximum slew rate of 0.5 deg/sec.

In the measurements, the antenna was moved at a nominal spacecraft-tracking rate, equivalent to a sidereal rate of 0.004 deg/sec in the azimuth coordinate. As indicated in Fig. 12, comparison is done with DSS-65 (DOY 014 versus DOY 021, 1991) and DSS 15 (DOY 293, 1990). The result from DOY 293 indicates an imperceptible effect of antenna motion whereas the data from DOY 014 and 021 show some degree of degradation. However, the degradation is small enough that it can be attributed to daily variation in the measurements.

[5] T. A. Rebold, "Status of DSS 15 Radio Science System Tests for Galileo Gravity Wave Experiments," JPL Interoffice Memorandum 3933-90-82 (internal document), Jet Propulsion Laboratory, Pasadena, California, June 25, 1990.

E. Radio Frequency Interference

1. With radar. Testing on DOY 272, 1990 overlapped with the Goldstone Solar System Radar experiment at DSS 14. Figure 13 clearly shows the impact of the nearby RFI. The period during which large phase bursts occurred correlated exactly with the transmission time of the 400-kW radar transmitter at 8495 MHz. Despite the fact that the radar signal was 95 MHz away from the 8400-MHz test signal, its effect was detrimental.

2. With dual-signal reception. For earlier measurements, both one-way and two-way measurements were made at the same time. That is, signals from both the ×84 signal generator and the test translator were simultaneously injected into the X-band maser. They were set at about 50 to 100 Hz apart, a separation that was considered wide enough to minimize the interference, yet close enough to have both signals inside the bandwidth of the last filter in the system. The rationales for dual-signal testing were to minimize the required test time and to enable a direct comparison between one-way and two-way measurements under the same conditions. It was later learned that there was intermodulation between the two signals that could not be eliminated by the 1-Hz lowpass filter used in data processing. Such a degradation can be seen in Figs. 14(a) and 14(b) in terms of the phase and Allan deviation, respectively, for DOY 087, 1992 testing.

F. Weather Effects

1. Impact of winds. Under strong wind conditions, antenna structural resonance may occur which would affect the equipment housed in the antenna cone. Different wind conditions were observed over the span of two-year testing. The worst case experienced was gusty winds up to 45 mph. Nevertheless, no correlation was seen between wind speed and stability degradation.

2. Impact of temperature. In order to study the impact of temperature on the 300-MHz IF cables that connect the antenna and the SPC area, an attempt was made to correlate the ambient temperature and the detected signal phase. This ambient temperature was measured by the DSCC Media Calibration (DMD) Subsystem. Although

the DMD temperature did not accurately reflect the temperature at the trench through which the cables ran, the result showed a correlation between the DMD temperature and the phase variation.

Five different data sets (DOY 035, DOY 027, DOY 114, DOY 105, and DOY 087) were used for this particular study. Any linear phase drift was first removed from the data set. This removal was necessary because any constant frequency offset caused by the inaccurate estimation of the input frequency would result in a linear phase drift. Unfortunately, by removing linear phase drift, any phase drift caused by thermal conditions that had the similar characteristic was also removed. Therefore, it was also necessary to fit the temperature with a linear function, and the residual temperature was then used in the correlation.

Figures 15(a–e) show the variation of residual temperature and phase, as a function of time, for DOYs' 035, 027, 114, 105, and 087. There was an apparent correlation between the two sets of residuals, although the effect was offset in time. Figure 16 presents a better picture of correlation as the residual phase is plotted against the residual temperature. Samples from all five data sets are used. The correlation can be observed by examining the slope of the best-fit curve, which is about 5.46 deg of phase per deg C. This value agrees with an expected value of 5.4 deg of phase per deg C for the effect of temperature on the 300-MHz IF cables of typical 400-m length, calculated from a thermal coefficient of delay of 25 ppm/deg C and velocity of propagation 70 percent of the speed of light. This derived thermal coefficient of delay (TCD) is higher than expected, but well within the observed range for coaxial cables. It is also possible that other equipment contributes to the drift. If so, the derived TCD would be proportionally lower.

VI. Performance Versus Requirement

Table 3 presents the design specifications for different subsystems in the Radio Science System. The requirement for the stability of the whole system, 4.5×10^{-15} stability at 1000-sec integration, is based on the need to support the Galileo mission.[6] Excluding the contribution of FTS and ANT, the requirement to which the measurements presented in Section V are compared is 3.0×10^{-15}. With the exception of data on DOY 068, all measurements are less than the required 3.0×10^{-15} level.

How do the specifications for the FTS and ANT measure against the actual performance? As shown in Table 4, stand-alone stability measurements for the FTS, based on Calhoun and Law's work,[7] indicated that the subsystem performs well within its specifications. For the antenna, if one assumes that the stability of the 34-m HEF antenna at X-band is similar to that of the R&D 34-m antenna at DSS 13 at K-band, then the antenna contribution is 1.4 times (i.e., $\sqrt{2}$) greater than its allocation. However, the combined FTS and ANT for the actual measurements is still less than their combined allocation. Thus, one can reasonably say that the total system performance, including both the observables and nonobservables, meets its requirements.

VII. Conclusions

Several conclusions can be drawn regarding the performance of the Radio Science System at the 34-m HEF stations.

(1) The system, under both one- and two-way configurations, performed well within its specification. However, the phase profiles indicated several small glitches and periodic variations, the cause of which was not identified. For the current requirements, these peculiar features do not cause the system to be out of specification; however, they should be investigated if future requirements will be more stringent. In the absence of known hardware failures, consistency among measurements of different dates demonstated that system performance is reliable.

(2) Frequency-dynamic testing indicated that system performance varied greatly from day to day. Out of three sets of measurements, one showed no difference in stability compared to the frequency-static results, one was more than twice as unstable, and one exceeded the specification. More data need to be collected to fully characterize the system under this mode of operation.

(3) The secondary effects of antenna motion, in terms of stretching the RF cables, and the vibration that the motion imposed on the equipment, appeared to be minimal when it occurred at the sidereal tracking rate.

(4) System stability was found to be very sensitive to RF interference. Most notable was the interference from the nearby radar 400-kW transmitter at the 70-m antenna. The presence of other signals in the

[6] Support Instrumentation Requirements Document for the 1989 Galileo Project, 625-501, Rev. A, JPL D-476 (internal document), Jet Propulsion Laboratory, Pasadena, California, May 1988.

[7] See Footnote 2.

operating bandwidth, such as a second test signal, also degraded stability performance.

(5) Definite correlation between the signal phase and the ambient temperature was observed, indicating that the 300-MHz IF cables connecting the antenna and signal-processing center are sensitive to thermal effect. If such coaxial cables are to be replaced with fiber-optic cables in the future, stability performance is expected to improve.

Acknowledgments

The authors express their gratitude to the following individuals, without whose contribution this study would not have been possible. First, appreciation extends to Malcom Calhoun, Julius Law, and Paul Kuhnle from the Frequency and Timing Subsystem Group for providing the engineering model of the fiber-optic distribution assembly and for their tireless support in early testing. Secondly, the authors thank Diana Howell and Jim Weese for spending many working nights at Goldstone to complete the system performance tests. Percy Montoya's accommodation to urgent requests for data extraction from the original data record tapes is much appreciated. The authors also thank North Ham and Tom Rebold for their technical introduction to the Radio Science System. The measurements would not have been realizable without the great support of operations personnel at all three Deep Space Communications Complexes; thanks in particular to Len Litherland, Bob Jenkins, and Kevin Knights at DSCC 40; and Larry Bracamonte, Guy Kaufman, and Rich Overcash at DSCC 10.

Table 1. Comparison of Allan deviations among three different methods of data processing at DSS 15.

Test	Integration, sec	Allan deviation, x 10^{-15}		
		Complex demodulation	DPLL	Time interval
	1	229.0	157.0	220.4
DOY 177, 1991	10	19.5	28.16	68.52
11:13–15:07	100	8.60	10.73	22.04
	1000	2.81	5.665	6.852
	1	377.5	189.1	129.0
DOY 334, 1990	10	53.80	35.14	20.2
1:30–11:30	100	18.05	3.969	2.35
	1000	4.507	0.9240	0.795
	1	68.44	99.52	129.0
DOY 027, 1993	10	9.730	11.77	15.5
11:09–16:27	100	1.595	1.844	2.05
	1000	1.362	1.337	1.25

Table 2. Summary of measurements collected under different configurations.

Focus of study	DSS site	Test	Link configuration	Antenna configuration	Antenna reference	Frequency condition	Integration time, sec	Allan dev., $\times 10^{-15}$
Two-way stability under static condition	65	DOY 035, 1993 04:19–13:00 8.7 hr	2-way	S[a]	F[b]	S[c]	1 10 100 1000 3600	103.6 16.35 4.159 0.8725 3.808
	45	DOY 067, 1993 00:33–07:06 6.6 hr	2-way	S	F	S	1 10 100 1000 3600	114.5 21.70 3.221 0.7944 0.5218
	45	DOY 341, 1992 11:50–21:15 9.5 hr	2-way	S	F	S	1 10 100 1000 3600	236.1 28.01 3.383 0.2626 0.6796
	15	DOY 027, 1993 11:09–16:27 5.3 hr	2-way	S	F	S	1 10 100 1000 3600	99.52 11.77 1.844 1.337 2.995
	15	DOY 105, 1992 02:50–12:50 10.0 hr	2-way	M[d]	F	S	1 10 100 1000 3600	164.4 7.750 1.081 0.7304 0.5727
Contribution of TXR	15	DOY 032, 1993 time not available 4 hr	2-way without TXR	S	F	S	1 10 100 1000	130.0 14.8 2.21 0.754
	15	DOY 032, 1993 time not available 2 hr	2-way with TXR	S	F	S	1 10 100 1000	129.0 14.8 1.61 0.421
One-way stability under static condition	15	DOY 114, 1992 01:49–10:04 8.7 hr	1-way	M	F	S	1 10 100 1000	143.9 941.31 0.9063 0.4507
	15	DOY 087, 1992 12:45–22:25 2.4 hr	1-way	M	F	S	1 10 100 1000	142.2 24.70 2.460 0.2969
Two-way stability under dynamic condition	45	DOY 340, 1992 13:00–22:25 9.4 hr	2-way	S	F	D[e]	1 10 100 1000 3600	195.9 36.98 1.943 0.5771 0.8945
	15	DOY 019, 1991 05:08–07:59 2.8 hr	2-way	M	P[f]	D	1 10 100 1000 3600	119.5 23.41 5.706 1.985 0.3898

[a] Static (antenna configuration only).
[b] Fiber-optic link.
[c] Static (fixed).
[d] Moving.
[e] Dynamic (ramped).
[f] Phase-stabilized cable.

Table 2. (cont'd).

Focus of study	DSS site	Test	Link configuration	Antenna configuration	Antenna reference	Frequency condition	Integration time, sec	Allan dev., $\times 10^{-15}$
	15	DOY 068, 1991 03:25–07:35 4.1 hr	2-way	M	P	D	1 10 100 1000 3600	296.5 48.29 14.00 5.940 11.31
Stability with other, non-fiber-optic references	15	DOY 086, 1990 19:46–21:50 2.0 hr	1-way	S	H[5]	S	1 10 100 1000	356.0 31.6 3.43 4.20
	65	DOY 014, 1991 14:22–01:28 11.1 hr	2-way	S	P	S	1 10 100 1000 3600	93.73 15.09 1.951 1.708 0.2379
Impact of antenna motion	15	DOY 293, 1990 06:06–10:36 4.5 hr	2-way	Stationary	F	S	1 10 100 1000	130.0 17.0 2.2 0.24
	15	DOY 293, 1990 11:55–13:15 1.3 hr	2-way	Moving	F	S	1 10 100 1000	130.0 17.0 3.1 0.54
	65	DOY 021, 1991 13:35–21:55 8.3 hr	2-way	Moving	F	S	1 10 100 1000 3600	94.50 60.15 5.308 0.7061 0.5633
	65	DOY 014, 1991 14:22–01:28 11.1 hr	2-way	Stationary	P	S	1 10 100 1000 3600	93.73 15.09 1.951 1.708 0.2379
Impact of RF interference								
From radar	15	DOY 272, 1990 04:10–07:45 3.6 hr	1-way	S	P	S	Not analyzed for stability. See Fig. 13.	
From exciter/ translator	15	DOY 087, 1992 Single-signal 12:45–15:05 2.4 hr	1-way	S	F	S	1 10 100 1000	142.0 24.70 2.46 0.297
	15	DOY 087, 1992 Dual-signal 10:42–12:45 3.0 hr	1-way	S	F	S	1 10 100 1000	227.0 37.3 2.79 0.343

[5] Hard-line coaxial cable.

Table 3. Design specification of components in the system.

Subsystem	Allan deviation, x 10^{-15} (1000-sec integration time)
Measurables	
Exciter	1.8
Transmitter	1.0
Receiver	2.1
Microwave (2-way)	0.7
DSCC spectrum processor	0.1
Subtotal of measurables	3.0
Nonmeasurables	
Frequency and timing (2-way)	3.0
Antenna (2-way)	1.4
Subtotal of nonmeasurables	3.3
System total (rss)	4.5

Table 4. Stand-alone measurements on the stability of the frequency and timing and antenna subsystems.[a]

Integration period, sec	Frequency and timing, Allan deviation, x 10^{-15} (1-way)	Antenna, Allan deviation, x 10^{-15} (1-way)
1	200.0	280.0
10	40.0	100.0
100	8.0	12.0
1000	1.5	1.4

[a] Based on Footnote 3 and [4].

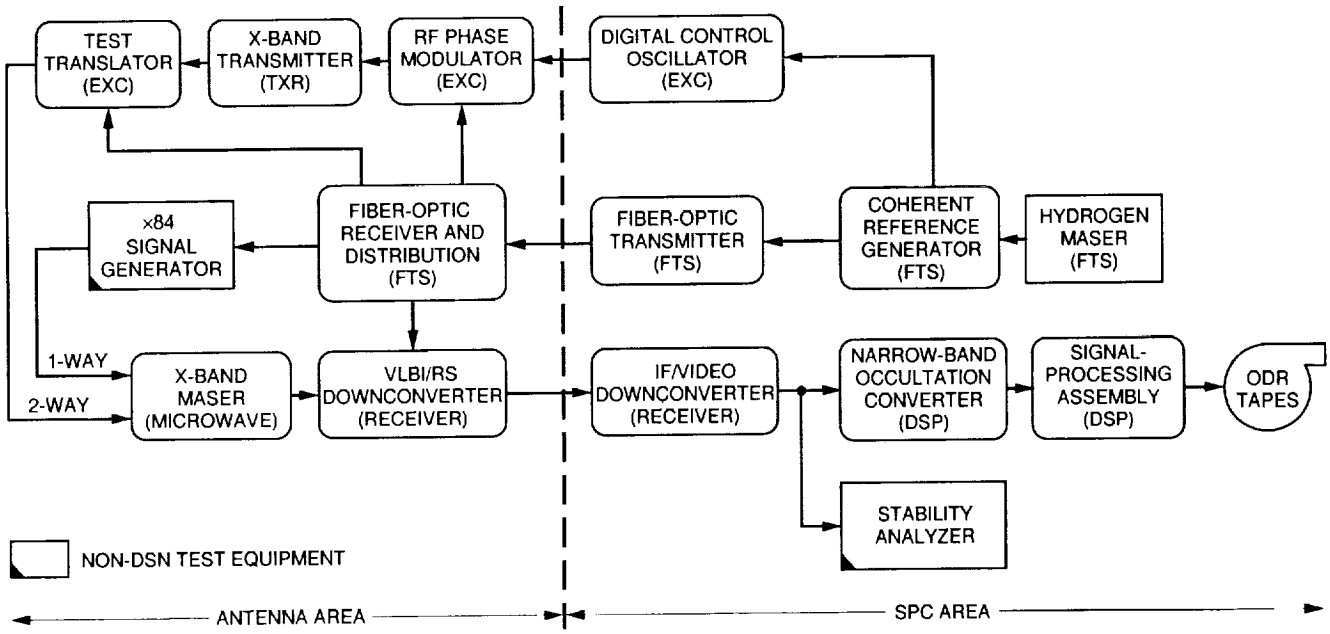

Fig. 1. Test configuration for stability measurements.

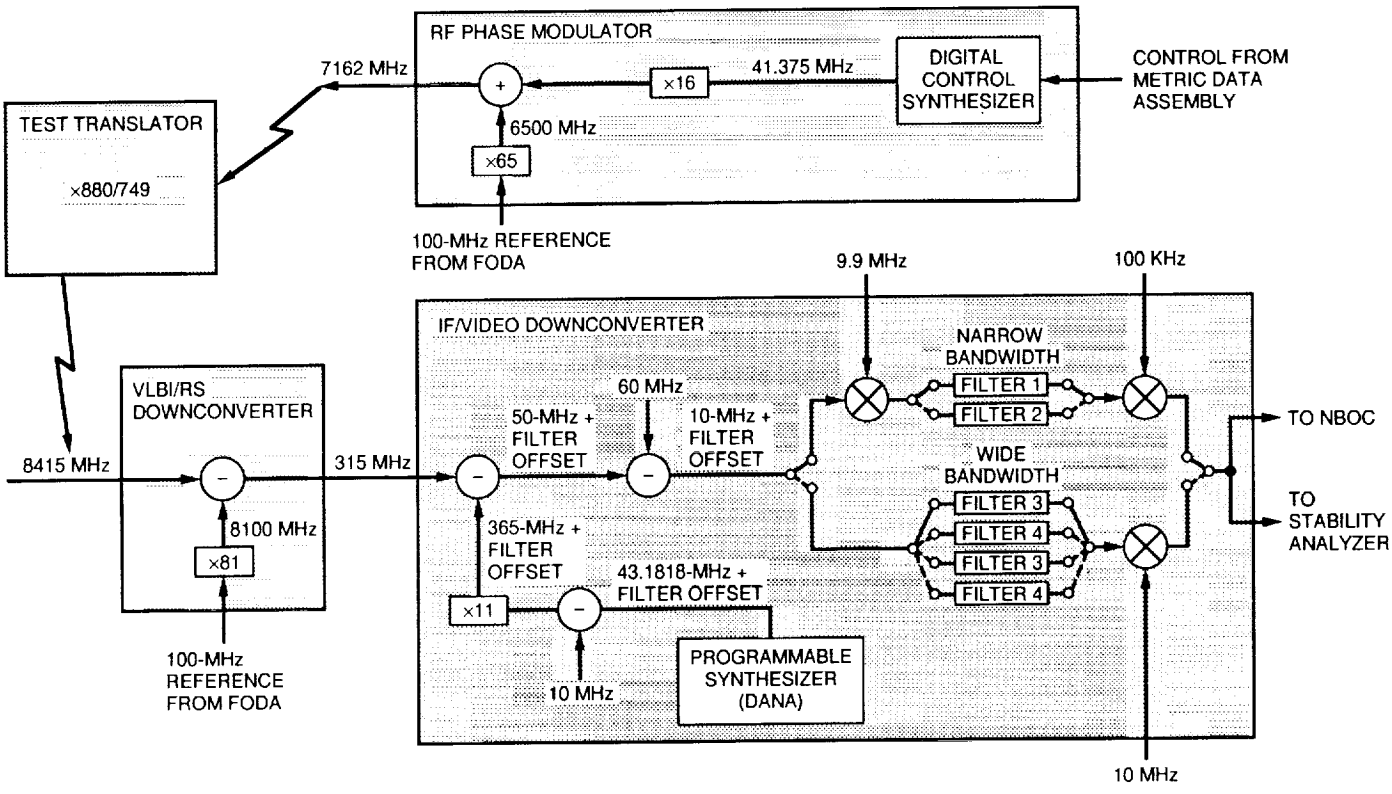

Fig. 2. Uplink and downlink frequency conversions.

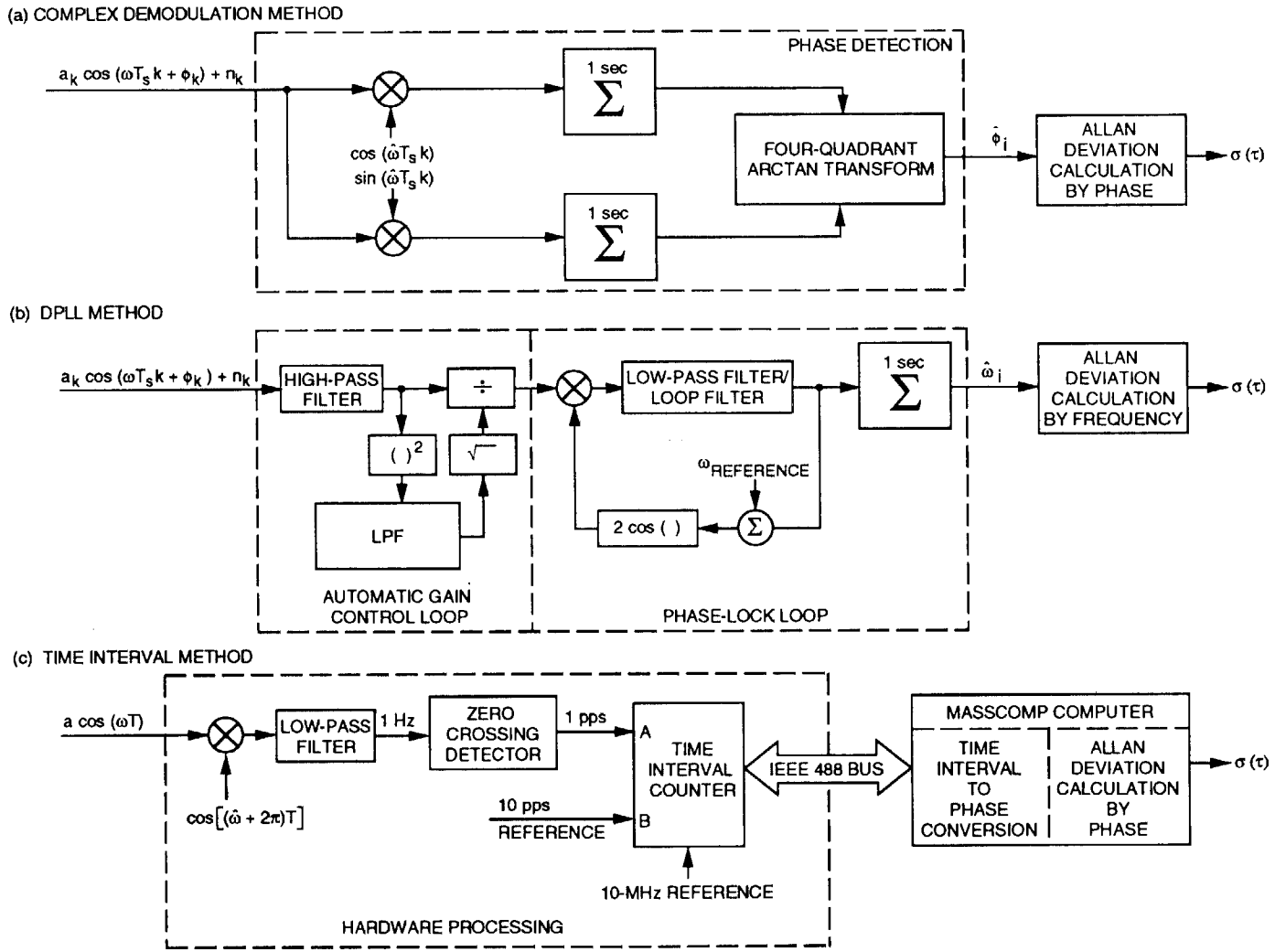

Fig. 3. Methods of data processing.

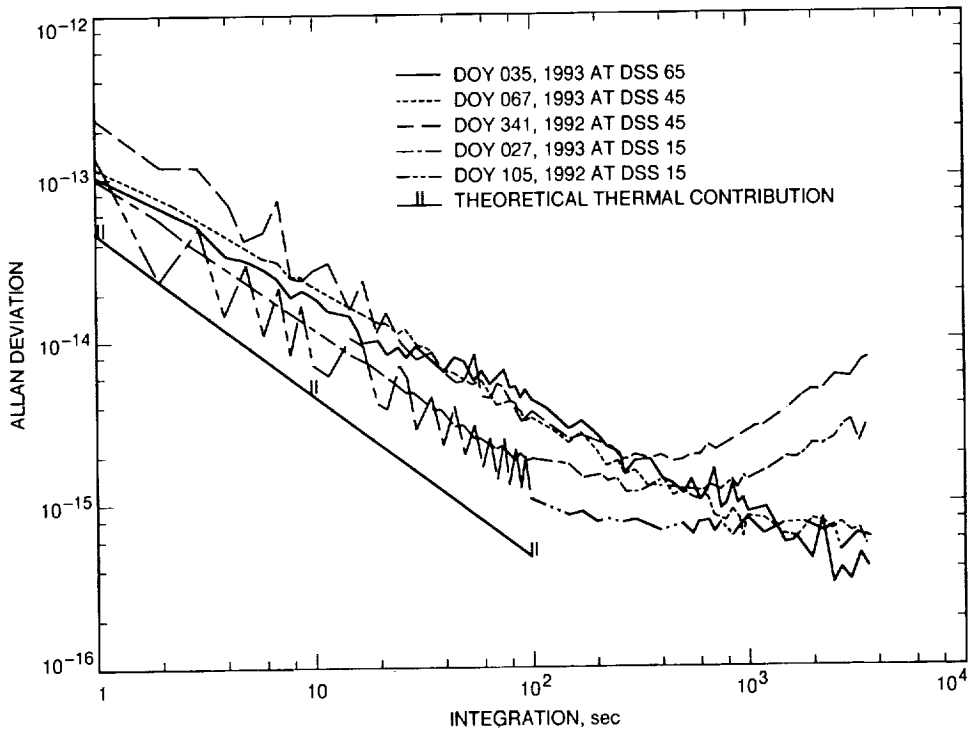

Fig. 4. Two-way stability with static frequency.

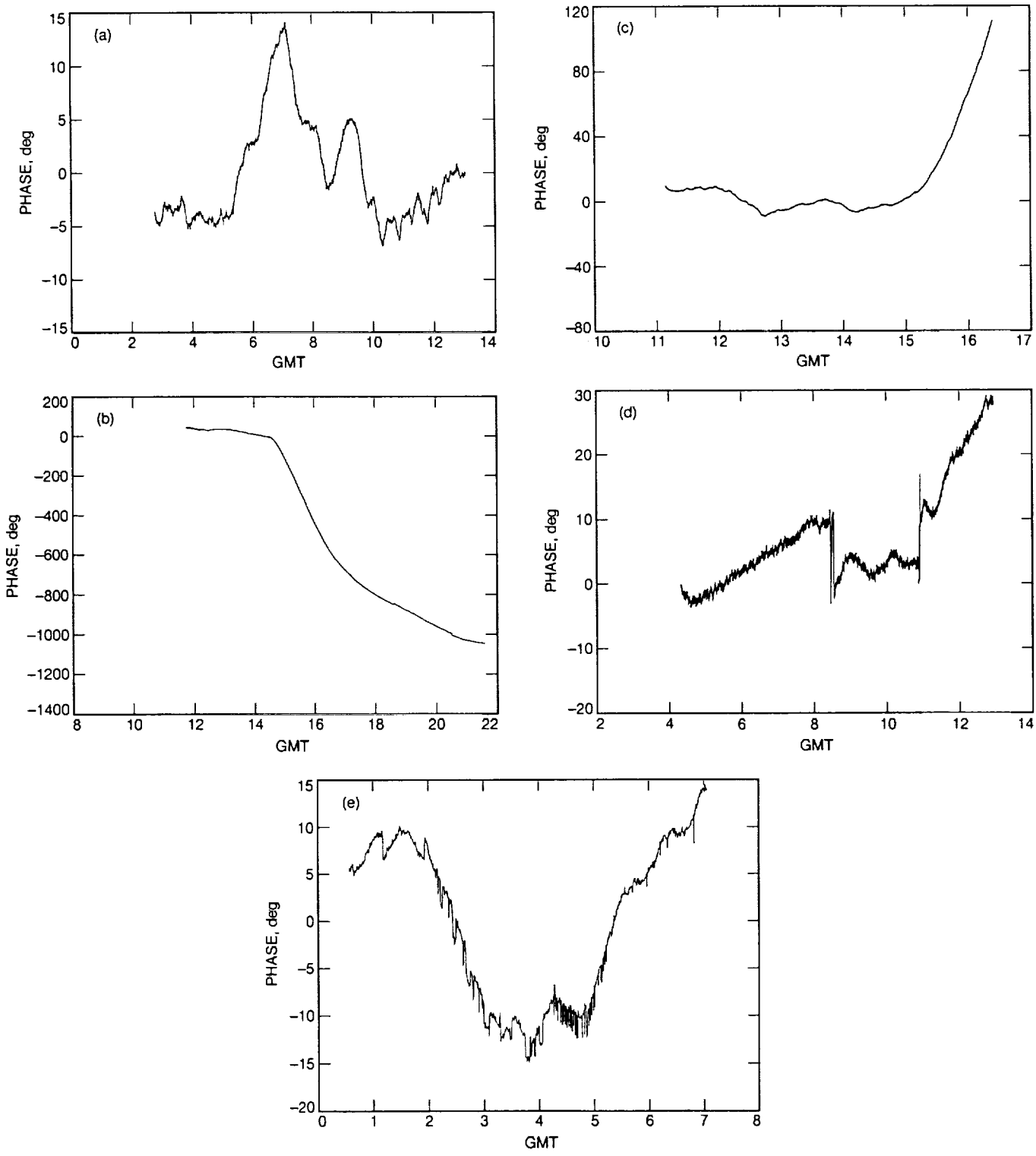

Fig. 5. Phase profiles for two-way frequency-static measurements: (a) DOY 105, 1992 at DSS 15; (b) DOY 341, 1992 at DSS 45; (c) DOY 027, 1993 at DSS 15; (d) DOY 035, 1993 at DSS 65; and (e) DOY 067, 1993 at DSS 45.

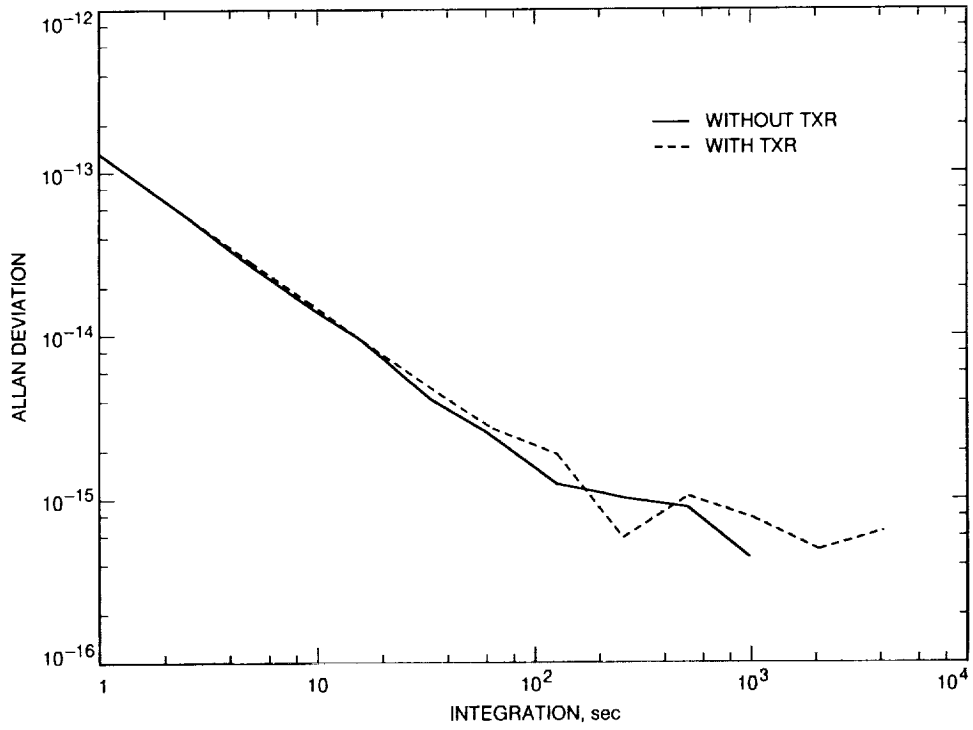

Fig. 6. Two-way stability with and without transmitter, DOY 032, 1993 at DSS 15.

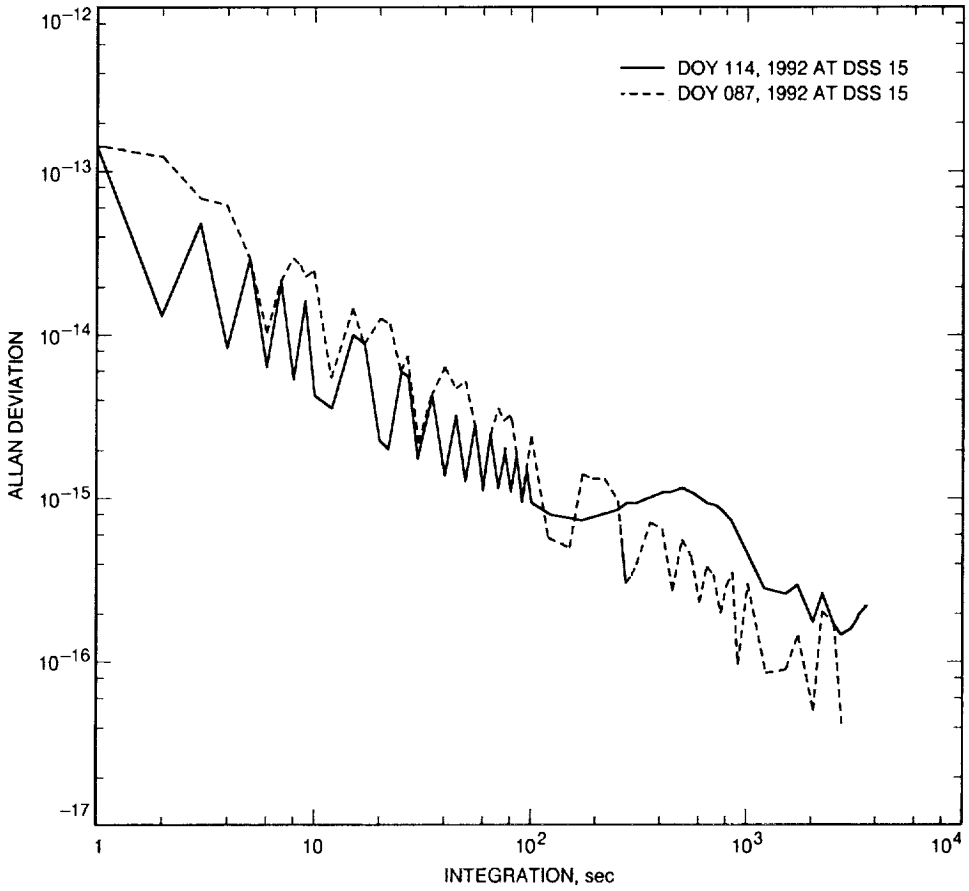

Fig. 7. One-way stability with static frequency.

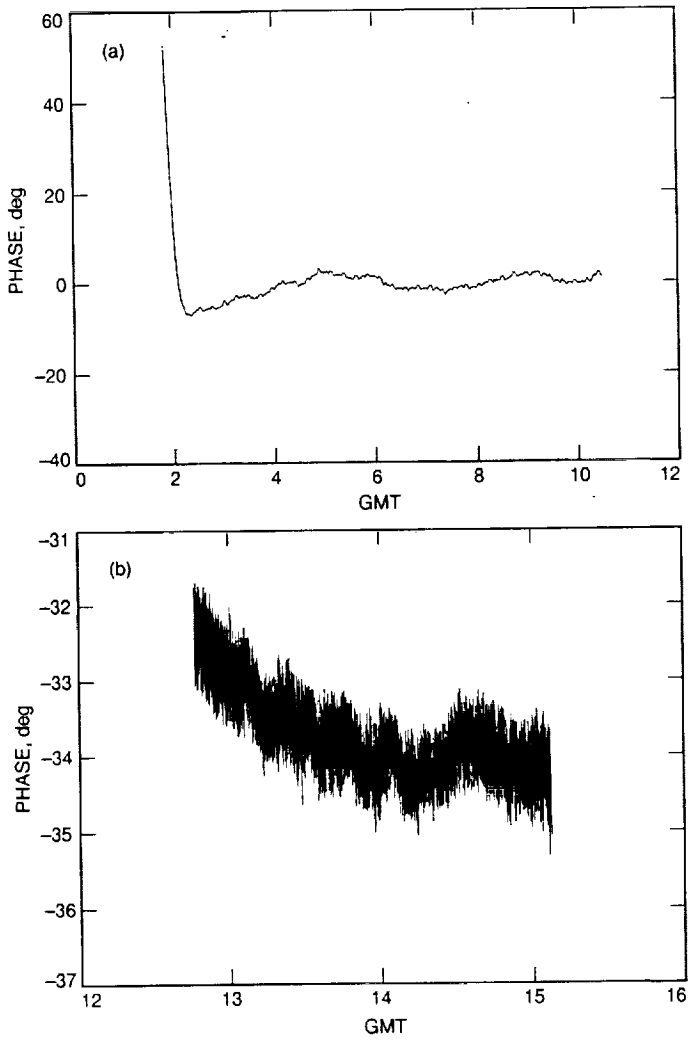

Fig. 8. Phase profiles for one-way frequency-static measurements at DSS 15: (a) DOY 114, 1991 and (b) DOY 087, 1992.

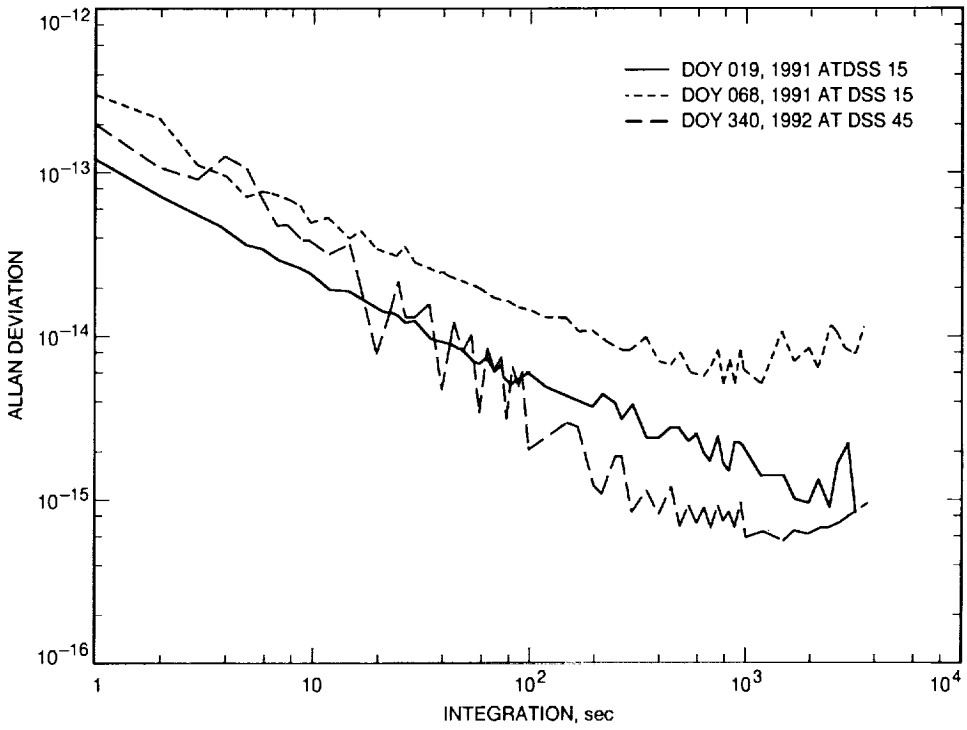

Fig. 9. Two-way stability with dynamic frequency.

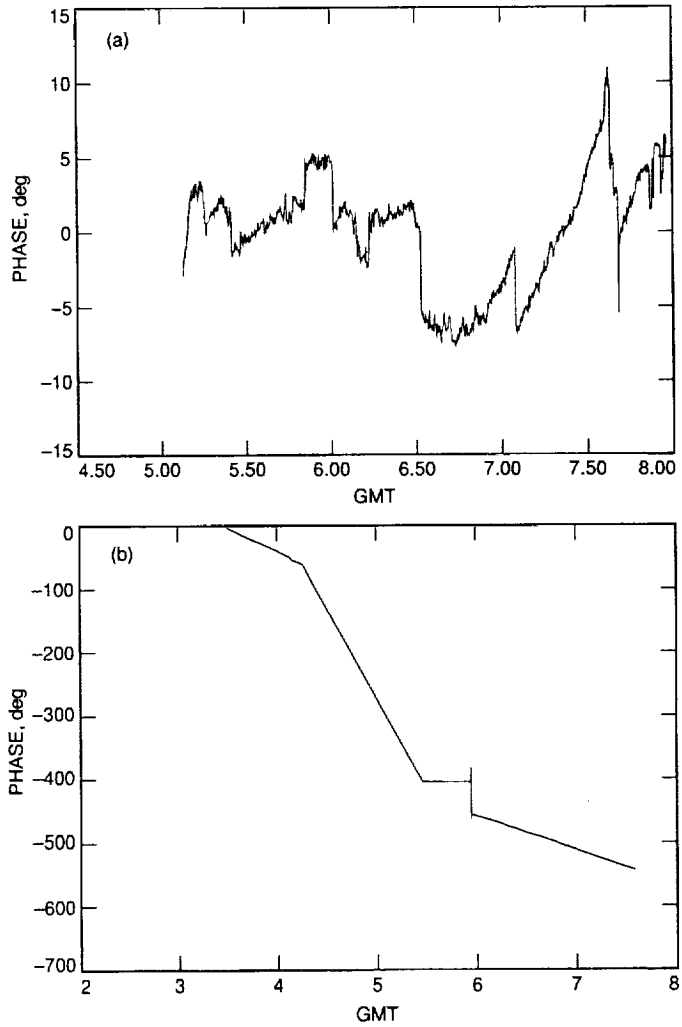

Fig. 10. Phase profiles at DSS 15: (a) DOY 019, 1991 and (b) DOY 068, 1991.

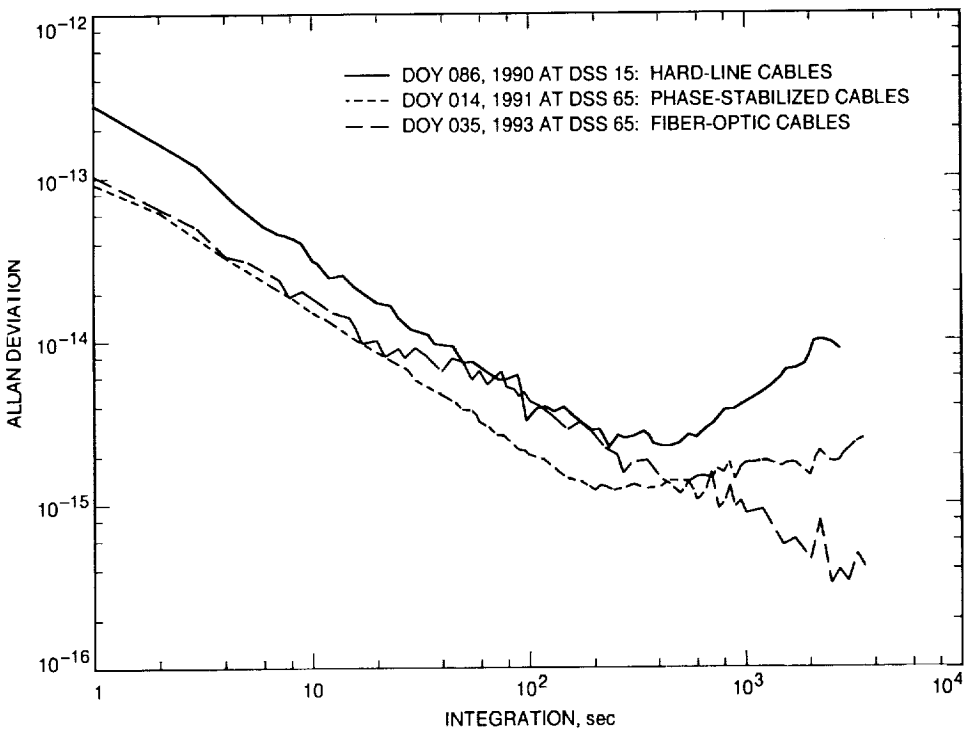

Fig. 11. Effect of antenna references.

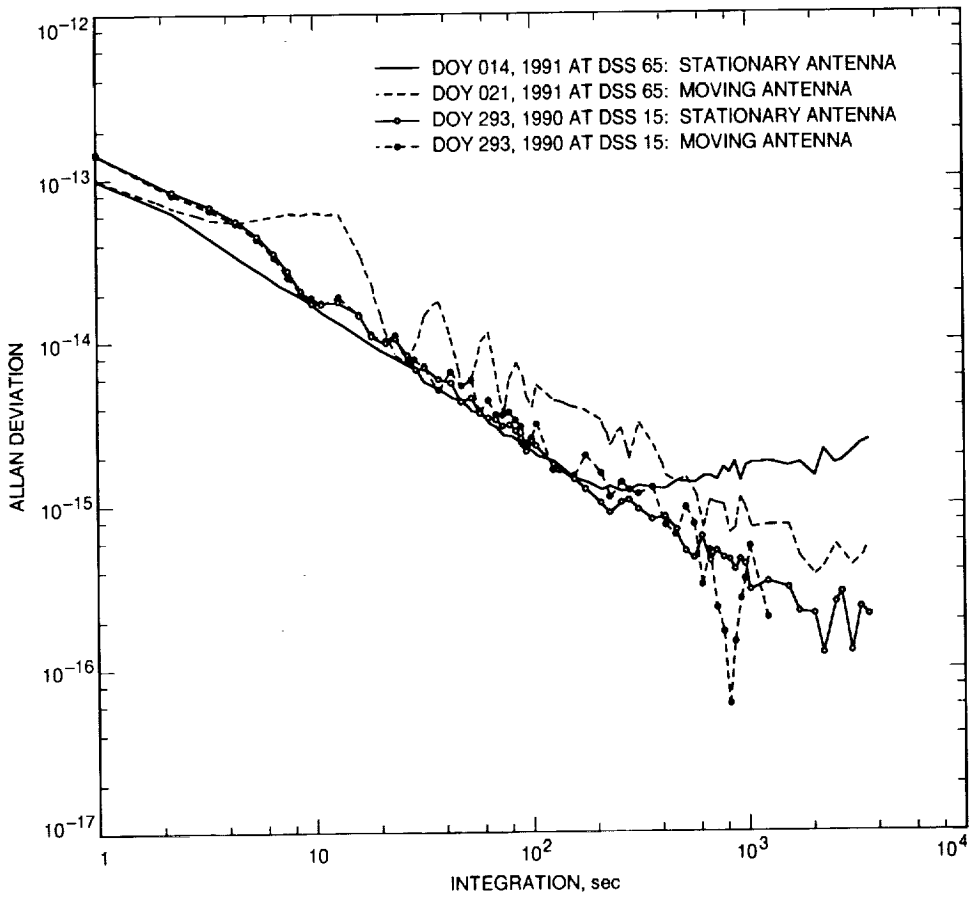

Fig. 12. Effect of antenna motion.

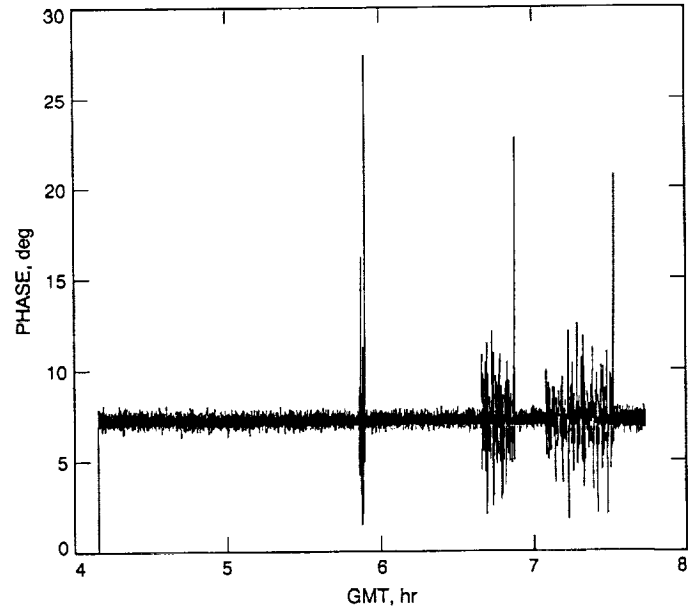

Fig. 13. Effect of RFI from radar transmission.

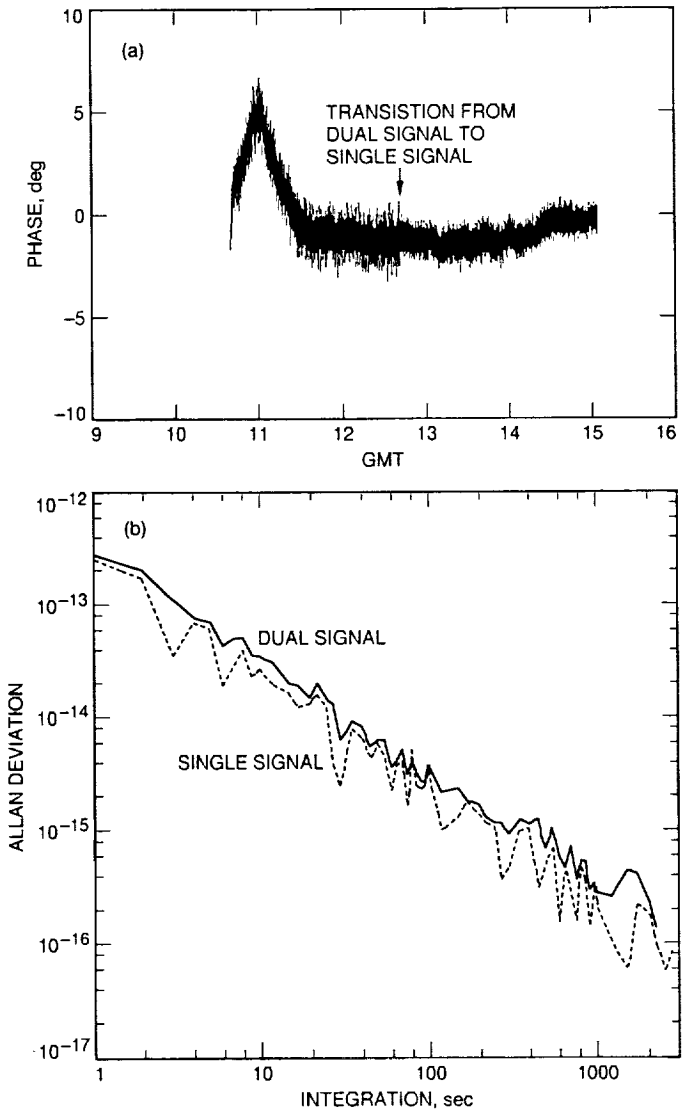

Fig. 14. Effect of RFI from dual-signal testing, DOY 087, 1992: (a) phase profile and (b) stability.

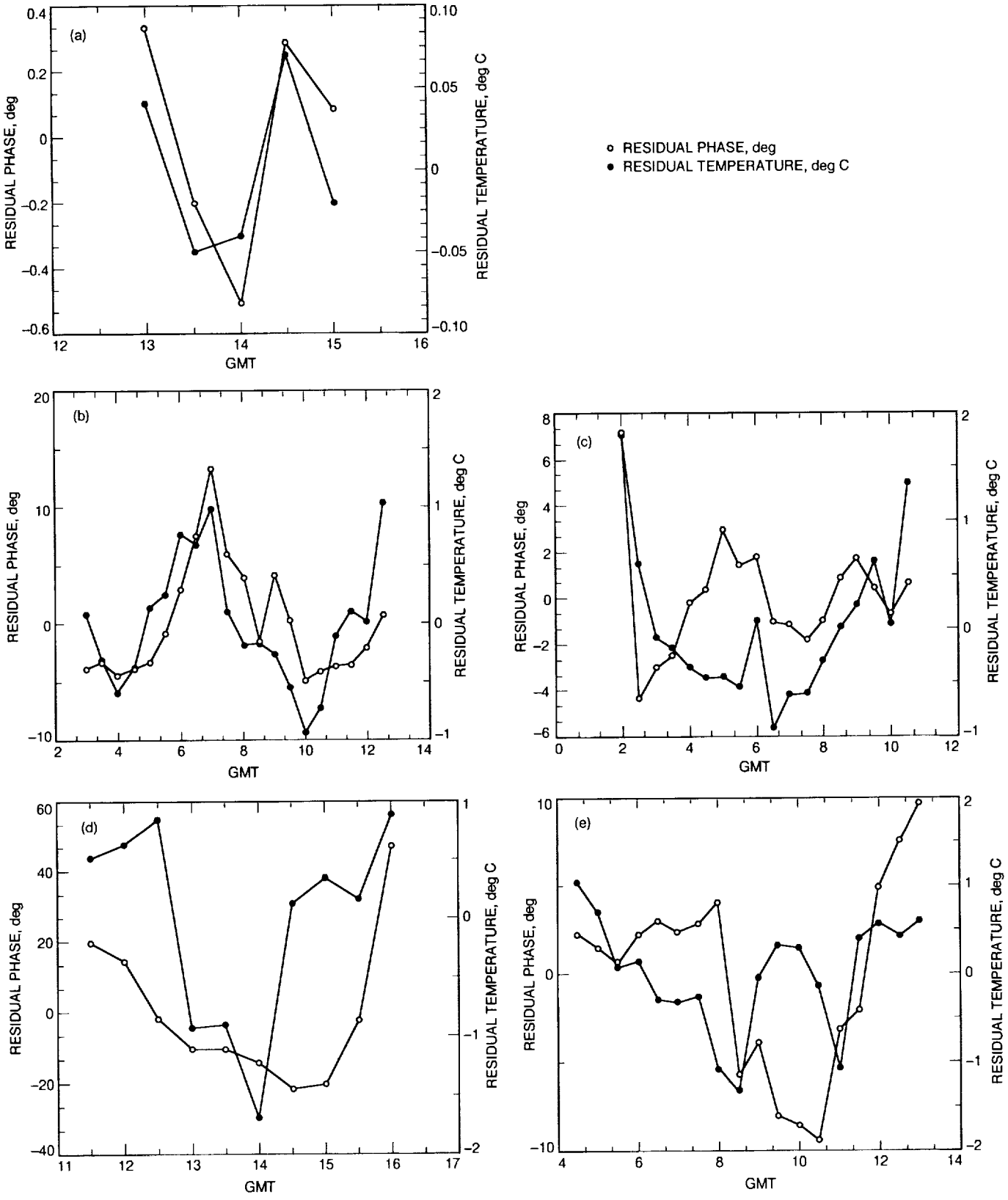

Fig. 15. Residual temperature and phase versus time: (a) DOY 087, 1992 at DSS 15; (b) DOY 105, 1992 at DSS 15; (c) DOY 114, 1992 at DSS 15; (d) DOY 027, 1993 at DSS 15; and (e) DOY 035, 1992 at DSS 65.

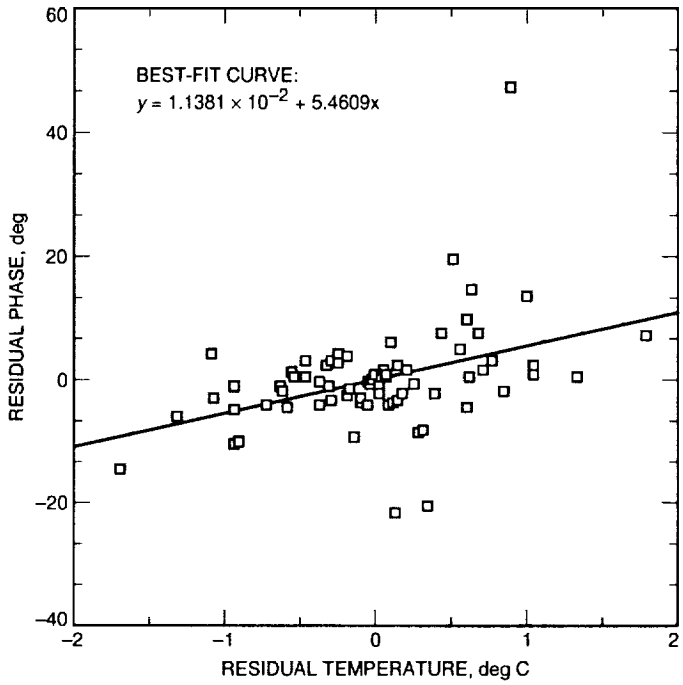

Fig. 16. Correlation of phase and temperature.